ELSEVIER

Journal of Photochemistry and Photobiology A: Chemistry 113 (1998) 243–250

Journal of Photochemistry and Photobiology A:Chemistry

Role of Cl^- adsorbed on silver-loaded zirconium phosphate for the photooxidation of OH^- to $OH^\bullet$

Hirokazu Miyoshi [a,*], Hiroki Kourai [b], Takuya Maeda [b], Tomio Yoshino [a]

[a] *Department of Radiological Technology, School of Medical Sciences, The University of Tokushima, 3-18-15 Kuramoto-cho, Tokushima 770, Japan*

[b] *Department of Bioscience and Technology, Faculty of Engineering, The University of Tokushima, 2-1 Minamijousanjima-cho, Tokushima 770, Japan*

Accepted 5 December 1997

Abstract

When a silver-loaded zirconium phosphate [$Ag_{1-x}H_xZr_2(PO_4)_3$] suspension was irradiated with a 500 W Xe lamp, the generation of $OH^\bullet$ was observed as the DMPO-OH using an ESR spin-trapping technique. The generation rate of DMPO-OH changed by adding various ions to the suspensions. The addition of Fe^{3+}, which has a redox potential of +0.771 V vs. NHE, increased the generation rate of DMPO-OH, indicating that the ion acted as an electron acceptor. In the presence of I^-, the generation rate of DMPO-OH decreased by oxidizing I^- with $OH^\bullet$. However, in the presence of Cl^-, the generation rate remarkably increased with the increase in the concentration of Cl^-. The quantum yield of the generation rate of DMPO-OH was about 10 times larger than that in the absence of Cl^-; at 400 nm from 0.36% to 2.7%, and at 500 nm from 0.037% to 0.41%. Such an effect of Cl^- could not be observed in the absence of $Ag_{1-x}H_xZr_2(PO_4)_3$. Furthermore, the generation rate of DMPO-OH during loading of Cl^- into the suspension showed a pH dependence with the maximal value at pH ca. 5.8. From a Lineweaver–Burk plot, K_m and $V_{max(DMPO\text{-}OH)}$ were determined to be 83.3 μmol dm^{-3} and 0.44 μmol dm^{-3} min^{-1}, respectively. These results suggested that the adsorption of Cl^- on the surface lead to the formation of an active site like a catalysis center in the enzyme. Cl adsorbed on a Zr atom not on a Ag atom in the surface region, because of the ca. 1 eV shift in binding energy at the peak of only $Zr_{3d5/2}$ in the XPS spectra of the Cl^--adsorbed $Ag_{1-x}H_xZr_2(PO_4)_3$. Consequently, the Cl^--adsorbed Zr atom on the surface was suggested to act as an electron pool in the photo-induced charge separation.

Keywords: Photooxidation; Silver-loaded zirconium phosphate; ESR; DMPO; Chloride ion

1. Introduction

The photoinactivation of photosystem II (PS II) has been extensively studied for a decade. Specially, Cl^--depletion and Ca^{2+}-depletion in PS II has been known to inhibit O_2 evolution [1,2]. Krieger and Rutherford [3] reported that Cl^--depleted PS II was more susceptible than Ca^{2+}-depleted PS II to damage by light. Thus, Cl^- plays an important role in O_2 evolution in PS II. In this study, it was found that in the presence of Cl^-, the photooxidation of OH^- to $OH^\bullet$ significantly proceeded in a silver-loaded zirconium phosphate [$Ag_{1-x}H_xZr_2(PO_4)_3$] suspension. In 1994, Kourai et al. [4,5] reported that $Ag_{1-x}H_xZr_2(PO_4)_3$ indicated the antibacterial property against *Escherichia coli* K12 W 3110 under visible light irradiation. It was important that the visible light irradiation and the *E. coli* contact the surface of $Ag_{1-x}H_xZr_2(PO_4)_3$. $Ag_{1-x}H_xZr_2(PO_4)_3$ was prepared from hydrogen zirconium phosphate [$HZr_2(PO_4)_3$] by the ion-exchanging of H^+ with Ag^+ at 3.7, 7, and 11 wt.%. Hydrogen zirconium phosphate has a three-dimensional skeletal structure composed of PO_4 and ZrO_6 [6]. As a photocathodic current was observed during visible light irradiation [7], a charge separation may occur on the surface of hydrogen zirconium phosphate. Therefore, the role of $Ag_{surface}^{+\bullet}$, which is a semi-reduced Ag^+ octahedrally surrounded by oxygen atoms, was suggested to a pool of electrons generated during the charge separation [7]. This was indicated by the XPS, FT–Raman, and ESR measurements. In fact, both $OH^\bullet$ (oxidation of OH^-) and $O_2^{-\bullet}$ (reduction of O_2) as the generated superoxide radicals were detected by the spin trap of 5,5-dimethyl-1-pyrroline-*N*-oxide [DMPO] [7]. On the other hand, the spin trap method with DMPO has been commonly used for the detection of the superoxide radicals such as $OH^\bullet$ and $O_2^{-\bullet}$. Recently, it was used to detect superoxide radicals generated in photochemical reactions with the TiO_2 photocatalyst in order to investigate the reaction mechanism of photogenerated holes and electrons in the homogeneous or

* Corresponding author. Tel.: +81-886-31-3111; fax: +81-886-33-7398; e-mail: miyoshi@medsci.tokushima-u.ac.jp

1010-6030/98/$19.00
PII S1010-6030(98)00198-1

heterogeneous phase by ultraviolet light irradiation [8–10]. In the case of TiO_2, it was found that the generated OH• was trapped with DMPO in the homogeneous phase, compared with the case of the irradiated H_2O_2 homogeneous system. In the heterogeneous phase, the reaction with OH• and DMPO was indicated to occur on the surface.

In this study, by using a spin-trapping technique, the influence of the added ions to the photogeneration of OH• was investigated. These adsorbed ions on $Ag_{1-x}H_xZr_2(PO_4)_3$ decreased or increased the generation rate of DMPO-OH. Especially, the adsorption of Cl^- and its remarkable increase in DMPO-OH were discussed based on the surface analysis by the potentiometric titration curve, XPS and FT-Raman techniques. Furthermore, from the change in the generation rate of DMPO-OH using added ions, which have various redox potentials, the energy diagram of $Ag_{1-x}H_xZr_2(PO_4)_3$ was estimated.

2. Experimental

2.1. Materials

Silver-loaded zirconium phosphates [$Ag_{1-x}H_xZr_2(PO_4)_3$] (Ag content: 3.7, 7, 11 wt.%) were provided by Toa Gousei. DMPO (LC-9130) and 2,2,6,6-tetramethyl-1-piperidine-*N*-oxyl nitroxide (TEMPO) were obtained from Labotec $Co(NH_3)_6Cl_3$ and $Ru(NH_3)_6Cl_3$ (reagent grade) were purchased from Aldrich Chemical. These reagents have been directly used in our investigations without further purification.

2.2. ESR measurement

Measurements of ESR spectra were performed using a JEOL TE-300 and ESPRIT-425 data system. Super oxide radicals were detected by a spin-trapping technique in the following manner. DMPO was used as the spin trap reagent. ESR spectra (X-band) of the DMPO adducts were measured with a JEOL DATUM LC12 quartz oblique cell for an aqueous solution. The concentration of DMPO-OH was determined by comparing the peak area of DMPO-OH to that of a 3.2 μmol dm^{-3} TEMPO aqueous solution as a standard in the respective ESR spectrum. After 0.4 or 0.2 cm^3 of a $Ag_{1-x}H_xZr_2(PO_4)_3$ powder suspension (1 mg cm^{-3}) was mixed with 0.005 cm^3 of the various ions such as KI, KBr, KCl, Na_2SO_4, KNO_3, $FeCl_3 \cdot 6H_2O$, $Fe(NO_3)_3 \cdot 9H_2O$, $Co(NH_3)_6Cl_3$, $Ru(NH_3)_6Cl_3$, and $K_3Fe(CN)_6$, 0.02 cm^3 of the DMPO spin trapping reagent (9.0 mol dm^{-3}) and added to the cell. The ESR spectra were measured during irradiation by a 500 W Xe lamp (Ushio, UI-501C) at room temperature with 8 mW power, 79 μT modulation width, Mn (II)/MgO external standard for g value, and ± 5 mT sweep width. The irradiation wavelength was selected to be 400, 500, 600, and 700 nm with cut-off filters (UV-37, Y-48, O-58, Toshiba Glass) and interference filters (KL-40, KL-50, KL-60, KL-70, Toshiba Glass). Quantum efficiencies of the generation of DMPO-OH at 400 and 500 nm were determined with 0.006 mol dm^{-3} and 0.15 mol dm^{-3} of Fe^{3+}-oxalato chemical actinometries.

2.3. Surface analysis

The XPS spectra of the $Ag_{1-x}H_xZr_2(PO_4)_3$ (Ag content 11 wt.%) powder and the Cl^--adsorbed ones were measured with a Shimadzu ESCA-1000AX. MgKα (1253.6 eV) was employed as the X-ray source. Data processing [11] was carried out with an HP 340 computer (Hewlett-Packard), which was attached to the Shimadzu ESCA-1000AX. The ESCA-1000AX was operated at 10 kV and 30 mA under a pressure of $10^{-6} \sim 10^{-7}$ Pa. The binding energy was corrected with $C_{1s} = 285$ eV from contaminant C. The sampling time was 200 ms and the repeat time was 20 for the $Ag_{3d5/2}$ peak. For another element, the repeat time was 1. The method of Savitzky and Golay [12] was used for the smoothing. The sample was modified to a pellet and attached to the sample probe with carbon tape.

Measurements of the FT-Raman spectra were performed with a Nihon Bunko NR-1800 at room temperature. The FT-Raman spectra of the $Ag_{1-x}H_xZr_2(PO_4)_3$ (Ag content 11 wt.%) and the Cl^--adsorbed ones were measured with an Ar ion laser (514.5 nm, 30 mW power) and a triple monochromomator. The sample powders were put on the glass plate and its surface was simply arranged with another glass plate: Ent. slit 500 μm, Sensitivity 1.0 (nA/FS) $\times$ 100, Scan speed 600 cm^{-1} min^{-1}, Accumulation 3.

The potentiometric titrations of OH^- and Cl^- were performed with the respective equipment. Sample of 0.1 g or 0.2 g $Ag_{1-x}H_xZr_2(PO_4)_3$ powder were suspended in 21 cm^3 of an aqueous solution containing 4.8 mmol dm^{-3} HNO_3 and 0.1 mol dm^{-3} KCl. After the pH meter (F-14, Horiba) was placed in the above suspension, 0.01 mol dm^{-3} NaOH was added to the suspension and the pH was measured. The amount of adsorbed OH^- was calculated from the difference in the amount of NaOH in the presence and the absence of the sample (0.1 g). The adsorption value per 1 g was then estimated. For the measurement of Cl^-, an Ion meter (Model Ti-8000, Toko Chemical Laboratories), which was connected with a reference electrode (MR 501DS, Toko) and a chloride ion electrode (5102, Toko) was used. After 1 g of $Ag_{1-x}H_xZr_2(PO_4)_3$ powder was suspended in 80 cm^3 of an aqueous solution prepared at pH 4.5, 5.8, and 6.1 using the acetate buffer solutions, the above two electrodes were placed in the solution. During the adding of the 1000 ppm NaCl aqueous solution to it, the electromotive force (e.m.f.) based on the Cl^- that remained in the solution was measured. The concentration of Cl^- was determined from the relation between e.m.f. and the concentration of Cl^-. The adsorption of Cl^- on the surface of the $Ag_{1-x}H_xZr_2(PO_4)_3$ was estimated from the subtraction between the added one and the remaining one.

3. Results and discussion

3.1. Change in the generation rate of DMPO-OH by added ions

When the silver-loaded zirconium phosphate [$Ag_{1-x}H_xZr_2(PO_4)_3$] suspension was irradiated by visible light, it was found that $OH^{\bullet}$ was generated on the surface using the ESR spin-trapping technique [7]. This $OH^{\bullet}$ is trapped with DMPO and DMPO-OH is formed. By loading the ions (0.005 cm^3) into suspensions containing 0.2 mg per 0.22 cm^3 of $Ag_{1-x}H_xZr_2(PO_4)_3$ (11 wt.% Ag content) and DMPO (0.8 mol dm^{-3}), the generation rate of DMPO-OH was changed. Fig. 1 shows the ESR spectra in the presence of various ions. As shown in Fig. 1a–e, a typical pattern of DMPO-OH, in which the height is 1:2:2:1 and the hyperfine splitting constant was $a_H = a_N = 1.49$ mT, were observed. The intensity decreased from Fig. 1a–e. The ESR spectrum of Fig. 1f shows a mixed spectra of DMPO-OH and DMPO-O_2^- [7]. As shown in Fig. 1, comparing with the peak area for DMPO-OH in the absence of ions (c), an increase (a,b) and a decrease (d,e,f) in the peak area for DMPO-OH in the ESR spectra were observed. The calculated concentration of DMPO-OH from the peak area is shown in Table 1. The reason why these phenomena occur is based on the following ideas.

Increase in the generation rate of $OH^{\bullet}$ on the surface or in the solution

(1) the effective charge separation (increase in reactive electron and hole).

(2) the increase in the active site.

Decrease in the generation rate of $OH^{\bullet}$ on the surface or in the solution:

(3) the reaction between the added ions and $OH^{\bullet}$

(4) the block on the active site.

The aforementioned ideas indicate the participation of the surface of $Ag_{1-x}H_xZr_2(PO_4)_3$ composed of Ag, Zr, and PO_4^{3-}. In the case of halogen ions such as I^- and Br^-, the generation rate of DMPO-OH changed with respect to their redox potentials. The redox potential and the reaction rate constant with $OH^{\bullet}$ are +0.535 V vs. NHE at pH 0 for I_2/I^- [13], $k = 1.0 \times 10^{10}$ (mol dm^{-3})$^{-1}$ s^{-1} at pH ~ 7 [14] and +1.065 V vs. NHE at pH 0 for Br_2/Br^- [13], $k = 1.1 \times 10^{10}$ (mol dm^{-3})$^{-1}$ s^{-1} at pH ~ 1 [14], respectively. Both ions can be oxidized by $OH^{\bullet}$ because of the higher redox potential than that of $OH^{\bullet}$ (for $OH^{\bullet}/OH^-$, $E^{\circ} = +2.7$ V vs. NHE at acid pH [14]) and their reaction rates with $OH^{\bullet}$ are very high. In addition to I^-, it was found that the spectrum was a mixed spectra (as shown in Fig. 1e) of DMPO-OH and DMPO-O_2^- by the simulating ESR spectra of DMPO-OH and DMPO-O_2^- [7]. This indicates that the adsorbed I^- was trapped with $OH^{\bullet}$. Therefore, the amount of $OH^{\bullet}$ did not increase and the $O_2^{-\bullet}$ could be detected. Photooxidation of I^- in a $Ag_{1-x}H_xZr_2(PO_4)_3$ suspension was investigated using the I_2–starch reaction. In the presence of I^- by visible light irradiation, I_2 was formed. However, an addition of I^-–starch solution to $Ag_{1-x}H_xZr_2(PO_4)_3$ suspension immediately after visible light irradiation (500 W Xe lamp with UV-33 cut-off filter) did not generate I_2. This means that I^- was adsorbed on the surface and oxidized by the photogenerated holes on the surface of $Ag_{1-x}H_xZr_2(PO_4)_3$. On the other hand, in the presence of Cl^-, the generation rate of DMPO-OH remarkably increased. This was a strange phenomenon, because the redox potential of Cl_2/Cl^- is +1.360 V vs. NHE at pH 0 [13] and the reaction rate with $OH^{\bullet}$ is $k = 4.3 \times 10^9$ (mol dm^{-3})$^{-1}$ s^{-1} at pH ~ 2 [14]. It is known that the reaction between $OH^{\bullet}$ (for $OH^{\bullet}/OH^-$, $E^{\circ} = +2.7$ V vs. NHE at acid pH [14]) and Cl^- occurred at pH 2 [14]. If $OH^{\bullet}$ and Cl^- reacted in this study, the generation rate of DMPO-OH must be decreased. From the radiolysis of water by ^{60}Co γ-rays (Dose: 1.29 C kg^{-1}) in air, the generated $OH^{\bullet}$ can be trapped with DMPO and its ESR signal appears. When I^-

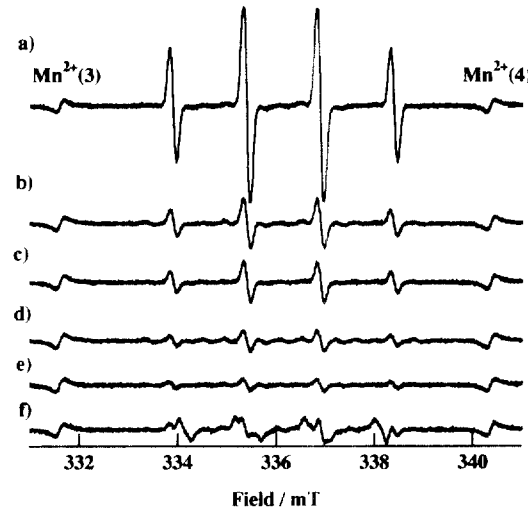

Fig. 1. The ESR spectra of DMPO-OH in the irradiated $Ag_{1-x}H_xZr_2(PO_4)_3$ suspension in the presence of various ions. (a) 1 mmol dm^{-3} Cl^-, (b) 0.06 mmol dm^{-3} SO_4^{2-}, (c) no ion, (d) 1 mmol dm^{-3} NO_3^-, (e) 1 mmol dm^{-3} Br^-, and (f) 1 mmol dm^{-3} I^-. A total of 200 μg of $Ag_{1-x}H_xZr_2(PO_4)_3$ was dispersed in 0.225 cm^3 of phosphate buffer solution at pH 5.8 containing 0.8 mol dm^{-3} of DMPO. Mn^{2+}(3) and Mn^{2+}(4) present for $g = 2.033$ and $g = 1.981$, respectively. Light source: 500 W Xe lamp with UV-37 cut-off filter. Irradiation time: 5 min.

Table 1
The influence of the added ions on the photogeneration rate of DMPO-OH in the irradiated $Ag_{1-x}H_xZr_2(PO_4)_3$ suspension

	Peak area	Concentration (μmol dm^{-3})
Cl^- [a]	744	4.5
Br^- [a]	41.2	0.25
I^- [a]	DMPO-OH + DMPO-O_2^-	
NO_3^- [a]	66	0.4
SO_4^{2-} [b]	190.2	1.2
No ions	136.8	0.83

[a] Concentration is 0.1 mmol dm^{-3}.
[b] Concentration is 0.06 mmol dm^{-3}.
Light source: 500 W Xe lamp with UV-37 cut-off filter; Irradiation time: 5 min.

was added to the aqueous solution, I^- ($k = 1.0 \times 10^{10}$ (mol dm^{-3})$^{-1}$ s^{-1}) traps OH$^\cdot$ in competition with DMPO ($k = 3.4 \times 10^9$ (mol dm^{-3})$^{-1}$ s^{-1} [15]). Thus the generation rate of DMPO-OH decreases. In the presence of Cl^-, the generation rate of DMPO-OH did not change. Cl^- could not trap OH$^\cdot$ in this solution at pH ~ 6. This certified that Cl^- and OH$^\cdot$ did not react at around neutral pH. This is the reason why the generation rate increase needs to be clarified. Otherwise, a decrease in the generation rate of DMPO-OH for NO_3^- and an increase in that for SO_4^{2-} were observed as shown in Table 1. These redox potentials and the reaction rate constants with OH$^\cdot$ are +2.45 V vs. NHE at pH 0 for $NO_3^\cdot/NO_3^-$, $k(HNO_3) = 1.4 \times 10^8$ (mol dm^{-3})$^{-1}$ s^{-1} [14] and +2.43 V vs. NHE at pH 0 for $SO_4^{\cdot-}/SO_4^{2-}$, $k(HSO_4^-) = 4.7 \times 10^5$ (mol dm^{-3})$^{-1}$ s^{-1} [14], respectively. These redox potentials and the reaction rate constants could not explain the behavior of the generation rate of DMPO-OH in the presence of these two anions. Therefore, in the case of NO_3^-, this anion would block the active site. Also, in the case of SO_4^{2-}, since it is reported that SO_4^{2-} specially adsorbed at the Ti^{4+} site on the surface of TiO_2 and the photocatalytic activity of TiO_2 decreased[16], SO_4^{2-} seems to be specially adsorbed on the surface of Zr atom in $Ag_{1-x}H_xZr_2(PO_4)_3$ and formed an active site in this case. The quasi-energy level of the photogenerated electron and hole were investigated as follows.

Fig. 2 shows the relation between the generation of DMPO-OH and irradiation time in the presence of various ions such as an electron acceptor. As shown in Fig. 2 the generation rate of DMPO-OH linearly increased with the irradiation time. When 187 μmol dm^{-3} of Fe^{3+} (■) as the electron acceptor was added to this system, the generation rate of DMPO-OH indicated a maximum value. The following was determined from the slope of each line in Fig. 2: 0.137 μmol dm^{-3} min^{-1} for 187 μmol dm^{-3} of Fe^{3+}, 0.037 μmol dm^{-3} min^{-1} for no ion, 0.036 μmol dm^{-3} min^{-1} for 118 μmol dm^{-3} of $Co(NH_3)_6^{3+}$, 0.033 μmol dm^{-3} min^{-1} for 11.8 μmol dm^{-3} of $Ru(NH_3)_6^{3+}$, and 0.004 μmol dm^{-3} min^{-1} for 118 μmol dm^{-3} of $Fe(CN)_6^{3-}$. Irrespective of the existence of Cl^- or NO_3^-, the behavior of the generation rate of DMPO-OH for the addition of Fe^{3+} was the same. This indicates that Fe^{3+} acts as an electron acceptor. Though it has been reported that Fe^{3+} interacted with DMPO in the dark and the DMPO-OH adduct was generated [17], in the concentration range of Fe^{3+} used in this experiment, such a DMPO-OH adduct was not detected in the dark. Fig. 3 shows the relation between the generation rate of DMPO-OH, which was obtained from the data of Fig. 2, and the redox potentials of the added ions. A linear relationship for them was recognized. Though the redox potentials are +0.058 V vs. NHE for $Co(NH_3)_6^{2-/3-}$ and +0.1 V vs. NHE for $Ru(NH_3)_6^{2+/3+}$ [13], in their presence, the generation rate of DMPO-OH almost did not increase. In the case of $Fe(CN)_6^{3-}$ (For $Fe(CN)_6^{4-/3-}$, $E = +0.361$ V vs. NHE [13]), it would adsorb on zirconium phosphate and prevent the adsorption of OH^-. Considering these redox potentials,

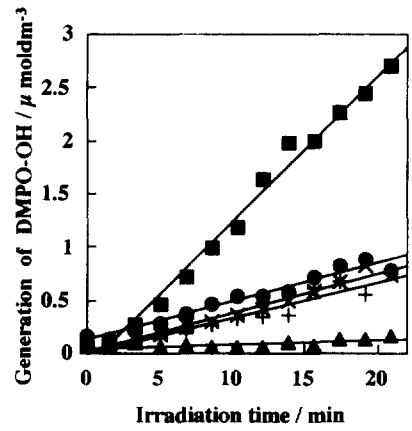

Fig. 2. The plot of generation of DMPO-OH vs. irradiation time in the irradiated $Ag_{1-x}H_xZr_2(PO_4)_3$ suspension in the presence of various ions. A total of 187 μmol dm^{-3} Fe^{3+} (■), no ion (●), 118 μmol dm^{-3} $Co(NH_3)_6^{3+}$ (×), 11.8 μmol dm^{-3} $Ru(NH_3)_6^{3+}$ (+), 118 μmol dm^{-3} $Fe(CN)_6^{3-}$ (▲). A total of 200 μg of $Ag_{1-x}H_xZr_2(PO_4)_3$ was dispersed in 0.425 cm^2 of phosphate buffer solution at pH 5.8 containing 0.4 mol dm^{-3} of DMPO. Light source: 500 W Xe lamp with UV-37 cut-off and 500 nm interference filters.

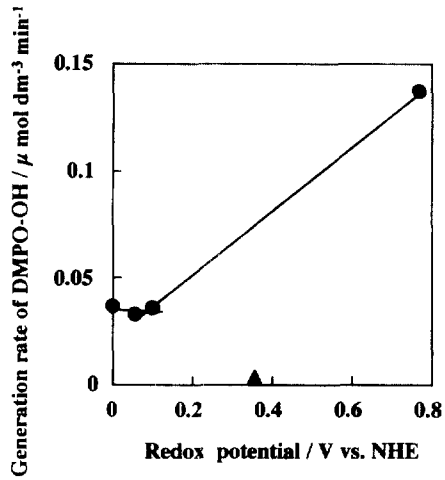

Fig. 3. The plot of generation rate of DMPO-OH vs. redox potential (vs. NHE). The generation rate was calculated from the data of Fig. 2. Fe^{3+}: 0.137 μmol dm^{-3} min^{-1}, no ion: 0.037 μmol dm^{-3} min^{-1}, $Co(NH_3)_6^{3+}$: 0.036 μmol dm^{-3} min^{-1} $Ru(NH_3)_6^{3+}$: 0.033 μmol dm^{-3} min^{-1}, $Fe(CN)_6^{3-}$: 0.004 μmol dm^{-3} min^{-1} (▲).

it seems that the ion with a low redox potential was effective in increasing the generation rate of DMPO-OH. Since the charge separation occurred on the zirconium phosphate, their ions would work as an electron acceptor on the surface. This means that a photogenerated electron on the surface would be scavenged by the added ions. Furthermore, considering the generation rates of DMPO-OH in the presence of $Co(NH_3)_6^{3+}$, $Ru(NH_3)_6^{3+}$, and in the absence of ions, these values were almost the same values. This indicates that the quasi-energy level of the photogenerated electron is ca. +0.1 V vs. NHE at pH 5.84 as shown in Fig. 3. Therefore, the quasi-energy level of the photogenerated hole is calculated to be ca. +2.17 V vs. NHE at pH 5.84 from the onset wave-

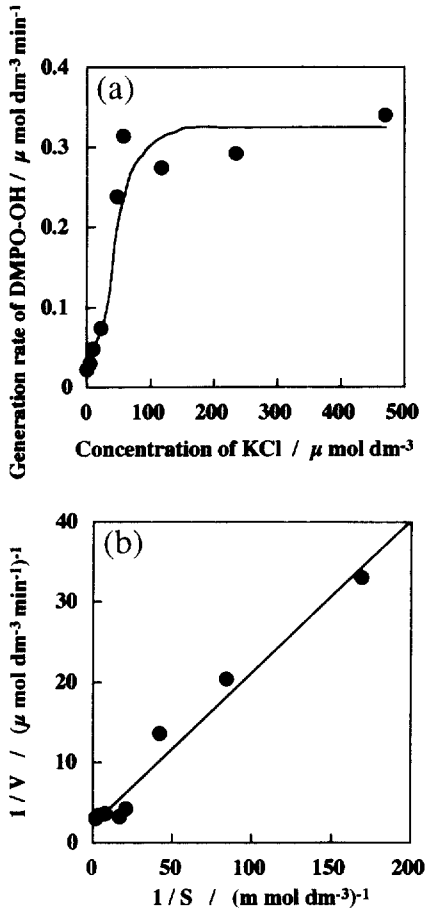

Fig. 4. Plot of generation rate of DMPO-OH vs. concentration of KCl in the irradiated $Ag_{1-x}H_xZr_2(PO_4)_3$ suspension 200 μg of $Ag_{1-x}H_xZr_2(PO_4)_3$ was dispersed 0.425 cm^3 of phosphate buffer solution at pH 5.8 contained 0.4 mol dm^{-3} of DMPO Light source: 500 W Xe lamp with UV-37 cut-off and 500 nm interference filters. (b) Reciprocal plot of Lineweaver–Burk using the data of (a).

length (600 nm = 2.07 eV) of the generation rate of DMPO-OH (see Fig. 8).

3.2. Adsorption of Cl^- on the surface and its influence on the generation rate of DMPO-OH

The increase in the generation rate of DMPO-OH by the addition of Cl^- as shown in Table 1 seems to be due to the formation of the active site, which was a complex between $Ag_{1-x}H_xZr_2(PO_4)_3$ and Cl^-. When the generation rate of DMPO-OH was plotted vs. the concentration of Cl^-, the saturation curve was obtained. Fig. 4a shows the relation between the generation rate of DMPO-OH and the concentration of added Cl^- at pH 5.8. The generation rate of DMPO-OH increased with the concentration of Cl^- and it reached saturation at ca. 118 μmol dm^{-3} as shown in Fig. 4a. This resembles the relation between the reaction rate and the concentration of substrate in the catalytic reaction based on the Michaelis–Menten equation.

$$E + L \rightleftarrows EL \quad (1)$$

where E is an OH^--adsorbed $Ag_{1-x}H_xZr_2(PO_4)_3$, L is Cl^-, and EL represents a complex between Cl^- and the OH^--adsorbed $Ag_{1-x}H_xZr_2(PO_4)_3$, which is an active site of the oxidation of OH^- to $OH^\bullet$ during irradiation. Since the amount of adsorbed OH^- is constant at pH 5.8, the factor that influenced the generation rate of DMPO-OH is only the concentration of added Cl^-.

$$EL \xrightarrow{h\nu} OH^\bullet + EL' \quad (2)$$

where EL′ presents a complex of Cl^- and an $Ag_{1-x}H_xZr_2(PO_4)_3$ without adsorbed OH^-. Considering only the concentration of EL, the concentration of EL decreased by releasing OH^- based on the oxidation of OH^- to $OH^\bullet$ during irradiation. Therefore, the generation rate of DMPO-OH ($V_{DMPO\text{-}OH}$) follows the Michaelis–Menten equation.

$$V_{DMPO\text{-}OH} = V_{max(DMPO\text{-}OH)}[Cl^-]/(K_m + [Cl^-]) \quad (3)$$

where $V_{max(DMPO\text{-}OH)}$ represents the maximum generation rate of DMPO-OH and K_m represents the Michaelis–Menten constant. Fig. 4b shows a Lineweaver–Burk plot for the concentration of Cl^- in order to obtain K_m and $V_{max(DMPO\text{-}OH)}$. A linear relationship was recognized. Therefore, a 1:1 interaction between Cl^- and OH^--adsorbed $Ag_{1-x}H_xZr_2(PO_4)_3$ was indicated and the active site for the photooxidation of OH^- to $OH^\bullet$ was formed. Value of $K_m = 83.3$ μmol dm^{-3} and $V_{max(DMPO\text{-}OH)} = 0.44$ μmol dm^{-3} min^{-1} were obtained. The K_m value (ca. 83.3 μmol dm^{-3}) was smaller than all Ag concentrations (maximum at ca. 1.0 mmol dm^{-3} for Ag 11 wt.% sample) on the surface. The newly formed active site due to the added ion is at a very low concentration. Furthermore, the generation rate of DMPO-OH in the presence of Cl^- was remarkably dependent on solution pH, and at pH

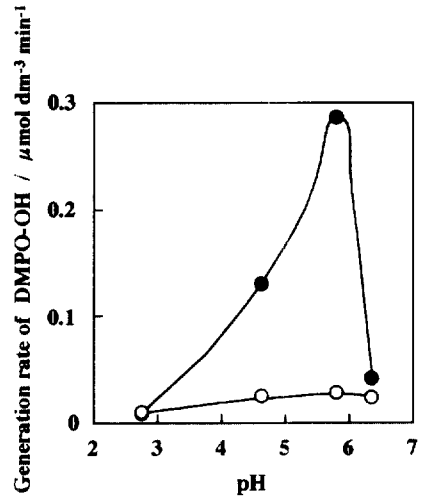

Fig. 5. pH dependence of the generation rate of DMPO-OH in the irradiated $Ag_{1-x}H_xZr_2(PO_4)_3$ suspension in the presence of 118 μmol dm^{-3} Cl^- (●) and in the absence of Cl^- (○). A total of 200 μg of $Ag_{1-x}H_xZr_2(PO_4)_3$ was dispersed 0.425 cm^3 of acetate buffer solution containing 0.4 mol dm^{-3} of DMPO Light source: 500 W Xe lamp with UV-37 cut-off and 500 nm interference filters.

5.8, it was a maximum as shown in Fig. 5. Though in the absence of Cl^- such behavior vs. solution pH was not observed, and the generation rate of DMPO-OH increased with the increase in the concentration of OH^-, i.e., the increase in pH, and was almost saturated at pH ca. 5.8. These behaviors were similar to that of an enzyme reaction, that is, based on solution pH, the ionization of the surface ion occurred. The relationship between solution pH and adsorption of Cl^- needs to be investigated. At pH 4.5, 5.8, and 6.1, the adsorption of Cl^- was investigated using an ion selective electrode. Fig. 6a shows the relation between the adsorbed Cl^- on 1 g of $Ag_{1-x}H_xZr_2(PO_4)_3$ powder and the added Cl^- at pH 4.5, 5.8, and 6.1 in the rage of 0 to 10 mg Cl^-. At pH 5.8, the amount of the adsorbed Cl^- vs. that of the added Cl^- was lower than that at pH 4.5 and 6.1. Fig. 6b shows the titration curves of an $Ag_{1-x}H_xZr_2(PO_4)_3$ (0.1 or 0.2 g) suspension in the presence of 0.1 mol dm^{-3} KCl. In the case of a 0.1-g sample, Cl^- seems to be fully adsorbed on the sample. As shown in Fig. 6b, OH^- in the solution adsorbed on the $Ag_{1-x}H_xZr_2(PO_4)_3$ and its amount increased with pH. From data in Fig. 6a and b, the amounts of adsorbed Cl^- and OH^- per 1 g $Ag_{1-x}H_xZr_2(PO_4)_3$ powder were calculated and shown in Fig. 6c. The adsorbed Cl^- decreased with an increase in adsorbed OH^- at pH 4.5 to 5.8. As shown in Table 2, the minimal adsorbed Cl^- and the maximal adsorbed OH^- were recognized at pH 5.8. Since the enhanced effect

Table 2
The adsorption of OH^- and Cl^- at respective pH

pH	Adsorption (μmol dm^{-3})[a]	
	OH^-	Cl^-
4.5	111	277
5.8	153	245
6.1	156	270

[a]Per 1 g of $Ag_{1-x}H_xZr_2(PO_4)_3$ powder.

occurred at pH 5.8, this indicates the optimal concentration of Cl^- on the surface. Though at pH 6.1, both the adsorbed OH^- and Cl^- increased, the generation rate of DMPO-OH decreased as shown in Fig. 5. This seems to be due to the ionization of the surface ion of $Ag_{1-x}H_xZr_2(PO_4)_3$. Fig. 7 shows the Raman spectra of these samples used in the experiment of Fig. 6a. As shown in Fig. 7, *labeled peaks at 124.5, 262.9, 293.4, 436.9, 597.3, 637.8, 1065.1, and 1086.6 cm^{-1} present the peaks based on zirconium phosphate [7]. The other peaks are due to $Ag_{surface}$–O and $Ag_{surface}$–O_2 vibrational frequencies [7]. These peaks in the Raman spectra in the range of 30 to 1300 cm^{-1} decreased with an increase in pH. At pH 6.1 the peaks observed at 30 to 400 cm^{-1} almost disappeared. Since $Ag_{1-x}H_xZr_2(PO_4)_3$ powder dissolves at a pH higher than 7, at pH 6.1 part of the skeletal structure seems to be ionized and dissolved on the surface. Therefore,

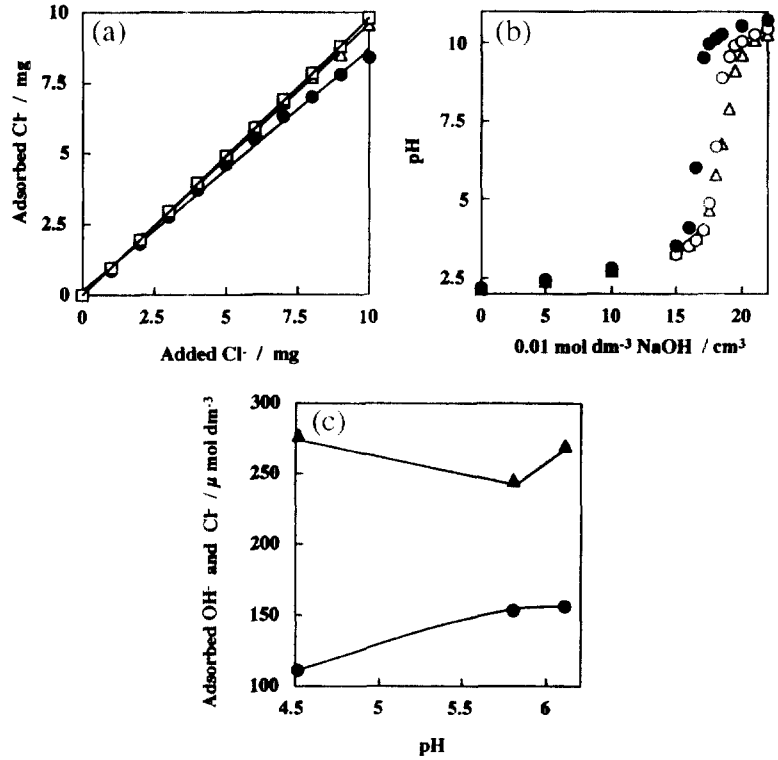

Fig. 6. (a) Plot of added chloride ion vs. adsorbed Cl^- on $Ag_{1-x}H_xZr_2(PO_4)_3$ powder in the acetate buffer solution at pH 4.5 (□), pH 5.8 (●), and pH 6.1 (Δ). After 1 g of $Ag_{1-x}H_xZr_2(PO_4)_3$ powder was suspended in the respective acetate buffer solution, 1000 ppm NaCl aqueous solution was added and e.m.f. was measured. (b) Potentiometric titration curves of the $Ag_{1-x}H_xZr_2(PO_4)_3$ suspended in 4.8 mmol dm^{-3} HNO_3 solution with 0.01 mol dm^{-3} NaOH solution. The amount of $Ag_{1-x}H_xZr_2(PO_4)_3$: 0.1 g(○), 0.2 g (Δ), and none(●) (c) pH dependence of the amount of Cl^- (▲) and OH^- (●) adsorbed on $Ag_{1-x}H_xZr_2(PO_4)_3$ powder. The adsorptions of Cl^- and OH^- were calculated from the data of (a) and (b).

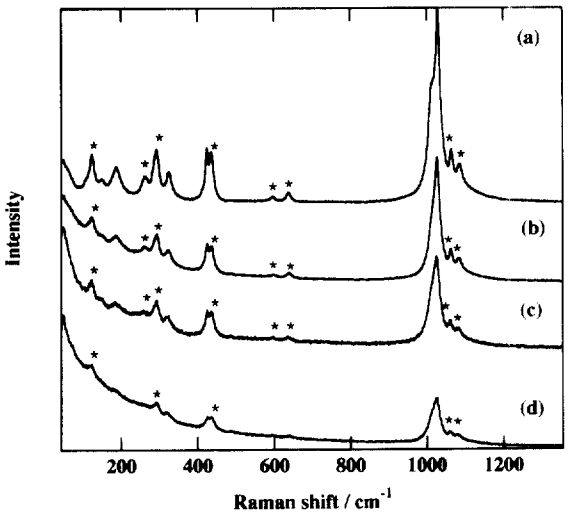

Fig. 7. Raman spectra of $Ag_{1-x}H_xZr_2(PO_4)_3$ powders. (a) standard, (b) pH 4.5, (c) pH 5.8, (d) pH 6.1 as shown in Fig. 6a in air at room temperature. The samples (b), (c), and (d) were obtained as a powder after the measurement of Fig. 6a. *Presents the peaks based on zirconium phosphate [7].

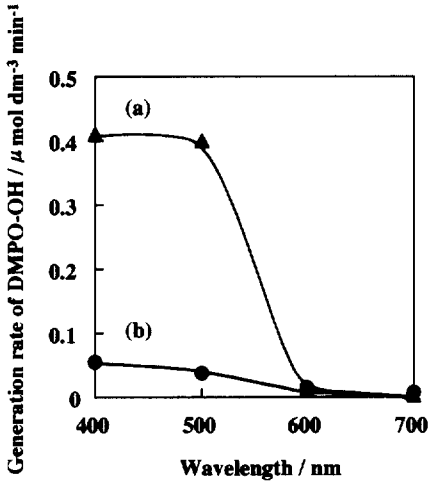

Fig. 8. Irradiation wavelength dependence of the generation rate of DMPO-OH in the irradiated $Ag_{1-x}H_xZr_2(PO_4)_3$ suspension in the presence of 118 μmol dm^{-3} Cl^- (a) and in the absence of Cl^- (b). 200 μg of $Ag_{1-x}H_xZr_2(PO_4)_3$ was dispersed in 0.425 cm^3 of phosphate buffer solution at pH 5.8 containing 0.4 mol dm^{-3} of DMPO. Light source: 500 W Xe lamp with cut-off and interference filters as shown in Section 2.

in spite of the increase in the adsorbed OH^- and Cl^-, the generation rate of DMPO-OH decreased.

The irradiation wavelength dependence of the generation rate of DMPO-OH in the irradiated $Ag_{1-x}H_xZr_2(PO_4)_3$ suspension in the presence of Cl^- (a) and no ion (b) is shown in Fig. 8. The onset wavelengths of both spectra were the same value of ca. 600 nm. The quantum efficiency of DMPO-OH was 10 times larger than that in the absence of Cl^- at 400 nm from 0.36 to 2.7%, and at 500 nm from 0.037 to 0.41%. Therefore, no new photoactive species formed and the generation of OH^* was promoted by Cl^- adsorption. For example, during the selective oxidation of ethylene to ethylene oxide at 523 K, the Cl atom plays an important role, in which the Cl atom as an electronic promoter interacts with the O-covered Ag surface (conduction electron) [18]. In our case, the site adsorbed by Cl^- would act as the electron pool [19] and make it effective for charge separation.

Table 3
The binding energies and atomic ratios on the surface of $Ag_{1-x}H_xZr_2(PO_4)_3$ determined by XPS

Cl^--adsorbed samples	Binding energies (eV)				Relative concentration		
	$Ag_{3d5/2}$	O_{1s}	P_{2p}	$Zr_{3d5/2}$	Ag/P	Zr/P	Ag/Zr
pH 4.5	368.4	531.6	133.5	433.7	0.1	0.39	0.25
pH 5.8	368.7	531.9	134.2	433.5	0.12	0.44	0.26
pH 6.1	368.5	531.8	133.8	433.4	0.07	0.37	0.19
Standard	368.8	531.9	134.1	434.6	0.08	0.34	0.23

To investigate the adsorption site, the XPS spectra of Ag, P, and Zr on $Ag_{1-x}H_xZr_2(PO_4)_3$ used in the experiment of Fig. 6a were measured. Table 3 shows the binding energies of $Ag_{3d5/2}$, P_{2p}, $Zr_{3d5/2}$, and O_{1s} and atomic ratios of Ag/P, Zr/P, and Ag/Zr. The binding energy of $Ag_{3d5/2}$ did not change but that of Zr shifted ca. −1 eV in the Cl^- adsorbed three pH samples compared with that of the standard shown in Table 3. This indicates that Cl^- adsorbs on the Zr of $Ag_{1-x}H_xZr_2(PO_4)_3$ and influences the electron state of Zr on the surface. In fact, after the potentiometric titration with NaCl, the sample became purple like the reduction of Ti^{4+} to Ti^{3+}. Consequently, the Zr atom would be easily reduced by the adsorbed Cl^- and the Cl^--adsorbed Zr atom would work as an electron pool like Ag metal [17]. Furthermore, since the atomic ratio of Ag/P, Zr/P, and Ag/Zr indicated a maximum value at pH 5.8, this pH also seemed to activate the surface of $Ag_{1-x}H_xZr_2(PO_4)_3$ by the ionization of the surface ion.

4. Conclusion

The addition of Cl^- to the silver-loaded zirconium phosphate suspension lead to the adsorption of Cl^- on the Zr atom on the surface. The relationship between this adsorption and the generation rate of DMPO-OH followed the Michaelis–Menten equation and the active center was formed. The generation rate of DMPO-OH was significantly increased and its quantum efficiency became about 10 times larger than that in the absence of Cl^-. The adsorption of Cl^- depended on the solution pH and at ca. pH 5.8, an adequate balance between the adsorptions of OH^- and Cl^- were produced. Furthermore, the atomic ratio of Ag/P and Ag/Zr on the surface becomes a maximum at this pH. On the other hand, in the case of I^-, I^- reacted with the photogenerated OH^* and the generation rate of DMPO-OH decreased, because OH^* forms from the oxidation of OH^- by the photogenerated positive hole. Fe^{3+}, $Co(NH_3)_6^{3+}$, and $Ru(NH_3)_6^{3+}$ acted as electron acceptors and the generation rate of DMPO-OH increased. As a result, the quasi-energy level of the photogenerated

electron was ca. +0.1 V vs. NHE and that of the photogenerated hole was ca. +2.17 V vs. NHE at pH 5.8.

Acknowledgements

We thank Toa Gousei of Japan for providing the zirconium phosphate samples and silver-loaded ones (Ag content 3.7, 7, and 11 wt.%) used in this work. The FT–Raman spectra were measured at the Center for Cooperative Research at Tokushima University. We also thank Dr. Shigeru Sugiyama for the ESCA measurement and useful discussion.

References

[1] C. Jegerschold, I. Virgin, S. Styring, Biochemistry 29 (1990) 6179.
[2] D.J. Blubaugh, M. Atamian, G.T. Babcock, J. Golbeck, G.M. Cheniae, Biochemistry 30 (1991) 7586.
[3] A. Krieger, A.W. Rutherford, Biochim. Biophys. Acta 1319 (1997) 91.
[4] H. Kourai, K. Nakagawa, Y. Yamada, J. Antibact. Antifungal Agents Jpn. (in Japanese) 21 (1993) 77.
[5] H. Kourai, Y. Manabe, Y. Yamada, J. Antibact. Antifungal Agents Jpn. 22 (1994) 595.
[6] J.B. Goodenough, H.Y.P. Hong, J.A. Kafalas, Mater. Res. Bull. 11 (1976) 203.
[7] H. Miyoshi, M. Ieyasu, T. Yoshino, H. Kourai, J. Photochem. Photobiol. A Chem., in press.
[8] H. Noda, K. Oikawa, H.O. Nishiguchi, H. Kamada, Bull. Chem. Soc. Jpn. 66 (1993) 3542.
[9] V. Brezova, A. Stasko, S. Biskupic, A. Blazkova, B. Havlinova, J. Phys. Chem. 98 (1994) 8977.
[10] M.A. Grela, M.E.J. Coronel, A.J. Colussi, J. Phys. Chem. 100 (1996) 16940.
[11] ESPAC 1000, User's Manual, Shimadzu.
[12] A. Savitsky, M.J.E. Golay, Anal. Chem. 36 (1964) 1627.
[13] A.J. Bard, R. Parsons, J. Jpordan, Standard Potentials in Aqueous Solution, Marcel Dekker, New York, 1985, pp. 77, 83, 90, 374, 408, 417.
[14] Z. Zuo, Y. Katsumura, K. Ueda, K. Ishigure, J. Chem. Soc. Faraday Trans. 93 (1997) 1885.
[15] E. Finkelstein, G.M. Rosen, E.J. Rauckman, Arch. Biochem. Biophys. 177 (1980) 1.
[16] P. Cuendet, M. Gratzel, J. Phys. Chem. 91 (1987) 654.
[17] K. Makino, T. Hagiwara, A. Hagi, M. Nishi, A. Murakami, Biochem. Biophys. Res. Commun. 172 (1990) 1073.
[18] X. Li, A. Vannice, J. Catal. 151 (1995) 87.
[19] A. Henglein, J. Phys. Chem. 83 (1979) 2209.